
PERFORMANCE COMPARISON OF 3D CORRESPONDENCE GROUPING ALGORITHM FOR 3D PLANT POINT CLOUDS

A PREPRINT

Shiva Azimi*

Department of Electrical Engineering
Indian Institute of Technology Delhi
New Delhi, India 110016
shiva.azimi@yahoo.com

Tapan K. Gandhi

Department of Electrical Engineering
Indian Institute of Technology Delhi
New Delhi, India 110016
tgandhi@ee.iitd.ac.in

September 4, 2019

ABSTRACT

Plant Phenomics can be used to monitor the health and the growth of plants. Computer vision applications like stereo reconstruction, image retrieval, object tracking, and object recognition play an important role in imaging based plant phenotyping. This paper offers a comparative evaluation of some popular 3D correspondence grouping algorithms, motivated by the important role that they can play in tasks such as model creation, plant recognition and identifying plant parts. Another contribution of this paper is the extension of 2D maximum likelihood matching to 3D Maximum Likelihood Estimation Sample Consensus (MLEASAC). MLESAC is efficient and is computationally less intense than 3D random sample consensus (RANSAC). We test these algorithms on 3D point clouds of plants along with two standard benchmarks addressing shape retrieval and point cloud registration scenarios. The performance is evaluated in terms of precision and recall.

Keywords Computer Vision · Correspondence Grouping · Plant Phenotyping · 3D Point Cloud

1 Introduction

Providing food to increasing world population has become a challenging task due to loss of arable land, climatic changes and many man made factors. This requirement for increasing the crop yield has necessitated the development of modern tools and techniques for increasing crop yield [1]. Plant phenotyping deals with the measurement of changes in phenomes in reaction to genetic and environmental changes and is an important plant science technique that can be used to monitor plant health and growth.

Recently, image-based high-throughput plant phenotyping has become an important computer vision research problem [2]. Measurements of visual plant features can be done using either two dimensional (2D) [3], [4] or three dimensional (3D) models [5] of the plant. However, since 3D models can capture much more information regarding the plant physiology as compared to 2D models, 3D models are preferred for plant phenotyping.

Finding correct correspondences between 3D shapes is a cornerstone in 3D computer vision tasks like 3D object recognition [6], point cloud registration [7], and 3D object categorization [8]. The first stage in local feature-based matching is detecting the keypoints on the surface and generating descriptors for every keypoints. Generating the vector feature descriptors surrounding each keypoint is computationally demanding, and thus, detecting keypoints is required to reduce the amount of computation required. In the second stage, crude initial matches are generated for marking the similarities between two 3D shapes. However, the initial matches have a high number of false positives due to reasons such as the residual errors from the proceeding steps like errors in keypoint localization, noise, point density variations, occlusion, overlaps, etc. To ensure accurate transformation estimation and hypothesis formulation, outliers must be filtered out from the initial matching, making correspondence grouping (CG) important [9].

*Corresponding author.

CG can play an important role in 3D model based plant phenotyping and automation of the farming process. Certain applications that require correspondence matching include creating 3D models, plant species recognition, recognition of plant parts, unsupervised template learning for fine-grained plant structures, etc. In autonomous farming also, techniques based on correspondence matching can be used in many ways. For instance, a general model of a harvesting machine can be produced in large numbers and then any farmer having no robotics skills can teach it on-site to identify and pick the required kind of fruit. In the same way, an autonomous weeding machine can be mass produced, then taught to distinguish weeds from the crops at different kinds of farms of widely, improving farming efficiency.

Although, there are studies in the existing literature comparing the performance of 3D CG algorithms [10], to the best of our knowledge, there is no work in the existing literature that deals specifically with the performance evaluation of the CG algorithms as applied to 3D point cloud data for plant health classification and plant growth analysis. Working with 3D point cloud data in the case of plants offers special challenges:

- Plants are made up of very fine structures that makes it very difficult to make a perfect scan. Thus the keypoint detectors local feature descriptors have to be robust to noise and holes present in the point cloud data.
- The lighting conditions in farming keep changing, offering different illumination conditions. This also changes the color and the texture of the plants, thus, making it very difficult to use the color information for decision making.

In summary, in this paper, we consider four most common 3D CG algorithms, viz, Nearest Neighbor Similarity Ratio (NNSR) [11], [12], Random Sample Consensus (RANSAC) [13], [9], Geometric Consistency (GC) [14], [15] and 3D Hough Voting (3DHV) [16], [17]. We have also implemented 3D MLEASAC, which combines Maximum Likelihood Estimation (MLE) and 3D RANSAC and is motivated by the approach taken in [18], [19] for 2D images. Fig.1 is represented the pipeline of our work.

The remainder of the paper is structured as follows. Section II briefly overviews the related work. We give a description of the 3DCG algorithms that we have considered for evaluation in Section III. performance evaluation is provided in Section IV. Finally, in Section V, we provide some perspectives and conclude the paper.

2 Related work

3DCG is still an active area in computer vision. 3DCG works based on local shape feature matching and is commonly used in other applications such as object recognition, pose estimation, point cloud registration, etc. Image based correspondences features have been explored in depth in the existing literature. Torresani [20] presented a method for finding correspondences between parse image features by graph matching. They solve the matching problem by minimizing a image matching objective function which depend on the appearance, geometric and spatial features. This method for real-world image matching is able to achieve global optimal by an unknown non-rigid mapping. Lowe [21] is described how to use SIFT features for object recognition in image. In this paper, they investigated Nearest Neighborhood algorithm for matching individual feature to a database of feature base on Euclidean distance of their feature vector. They found good matches in a large number of features with using distinctive descriptors. This method is extended to 3D in [9]. In [22] is modified RANSAC method for 3D object recognition and pose estimation. They obtained optimum number of iteration by using the combination algorithms of descriptor, hash table and RANSAC. In [14], Chen et al. used geometric constraints for 3DCG algorithm in 3D object recognition. They improved the version of Johnson et al. [23] algorithm for clustering the inliers into disjointed clusters. Tombari et al. [16] introduced 3D Hough Voting for 3D object recognition by using Hough Transform [24]. In the proposed approach each correspondence can cast a vote for presence of the unique reference point of object in the 3D Hough space simultaneously. Anders et al. [9] introduced two stage local and global method for casting a vote for finding 3DCG. On the local stage, they caste a vote for finding correspondences by geometric consistency and in the global stage, they cast a vote by covariance constraint. At the final stage, they compared their algorithm with existing ones.

3 3D correspondence grouping algorithms

In this section, we provide a brief overview the 3DCG algorithms. Given a model \mathcal{S} and a scene \mathcal{S}' , where an raw correspondence set \mathcal{C} is obtained after comparing the feature sets \mathcal{F} and \mathcal{F}' belongng to \mathcal{S} and \mathcal{S}' , respectively, the goal is to obtain a subset \mathcal{C}_{inlier} of \mathcal{C} that identifies the correct correspondences between \mathcal{S} and \mathcal{S}' , i.e., the inliers. An element in \mathcal{C} is given as: $c = \{p, p', s_{\mathcal{F}}(f, f')\}$, where p and p' are keypoints belonging to the model (source) and the scene (target), respectively, f and f' are the descriptors for these keypoints, and $s_{\mathcal{F}}(f, f')$ is the similarity score assigned to c . We now briefly explain the 3DCG algorithms considered in this paper.

3.1 Nearest neighbor similarity ratio

NNSR is a basic method for determining the initial correspondences [11]. This method is based on Lowe’s ratio [21]. It judges match features base on the ratio of two closest neighbors and obtained by Euclidean ($L2$) distance between an invariant feature vector $f \in \mathcal{F}$ with the nearest $f'_1 \in \mathcal{F}'$ and second nearest matching feature $f'_2 \in \mathcal{F}'$. A correspondence will be as an inlier if the Euclidean distance between f , f'_1 and f , f'_2 satisfies:

$$\frac{\|f - f'_1\|_{L2}}{\|f - f'_2\|_{L2}} \leq t_{nnsr}, \quad (1)$$

where, t_{nnsr} is the threshold. The NNSR will be used as a baseline for all comparison purposes.

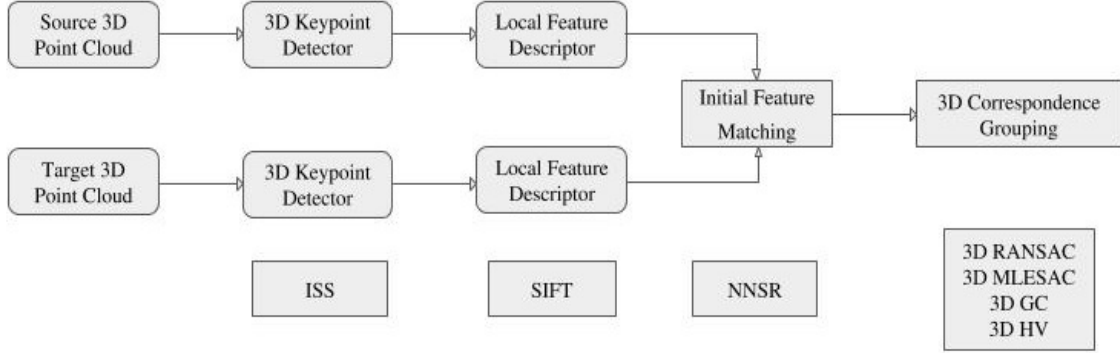


Figure 1: Performance comparison of 3D correspondence grouping algorithms

3.2 RANSAC

RANSAC is an iterative method for judging the correctness of a correspondence set by calculating the number of inliers returned in each iteration [13]. The RANSAC method uses random samples from the initial correspondences set \mathcal{C} in each iteration and finds the transformation T corresponding to those samples. The steps are repeated N_{ransac} iteration and the transformation is compared with a threshold t_{ransac} . The transformation returning the maximum number of inliers is judged the optimal T^* . The correspondences in \mathcal{C} that do not agree with T^* are classified as outliers.

3.3 Geometric consistency

CG method is based on geometric constrains for finding inliers and is not dependent on the local feature space [14]. The algorithm looks for consistency and compatibility in terms of consistent cluster. After finding initial matching set \mathcal{C} , we find the distance between keypoints from the seed in the model and scene and then we find $L2$ -distances between the pairwise correspondences to compare with the geometric constraint threshold t_{gc} . Finally, we choose the largest cluster as optimum one and classify the corresponding correspondences as inliers. The compatibility score for the given correspondences pair c_1 and c_2 is given as:

$$d(c_1, c_2) = |d(p_1, p_2) - d(p'_1, p'_2)| \leq t_{gc}, \quad (2)$$

where $d(p_1, p_2) = \|p_1 - p_2\|_{L2}$.

3.4 3D Hough voting

3DHV uses features by casting a vote in 3D Hough space for finding inliers [16]. In this method, after finding initial matching set \mathcal{C} , for each keypoint p_i in the source shape (model) that is in \mathcal{C} , the vector between source shape centroid C_S and p_i is computed in the global reference frame (GRF):

$$\mathbf{V}_{i,G}^S = C_S - p_i, \quad (3)$$

After that $\mathbf{V}_{i,G}^S$ is transformed to local reference frame (LRF), as we want our method to be translation and rotation invariant.

$$\mathbf{V}_{i,L}^S = \mathbf{R}_i^S \cdot \mathbf{V}_{i,G}^S, \quad (4)$$

Where \mathbf{R}_i^S is rotation matrix, and each line in \mathbf{R}_i^S being a unit vector of the LRF of p_i . Similarly, we can obtain $\mathbf{V}_{i,G}^{S'}$ corresponding to p'_i . Then, $\mathbf{V}_{i,L}^S = \mathbf{V}_{i,L}^{S'}$, because of the invariance in LRF. The vector $\mathbf{V}_{i,G}^{S'}$ is computed by transforming $\mathbf{V}_{i,L}^{S'}$ into GRF.

$$\mathbf{V}_{i,G}^{S'} = \mathbf{R}_i^{S'} \cdot \mathbf{V}_{i,L}^{S'} + p_i', \quad (5)$$

Eventually the feature f_i' could cast a vote in 3D Hough space through the vector $\mathbf{V}_{i,G}^{S'}$. The inliers correspond to the peak of Hough space.

3.5 3D MLESAC

MLESAC combines 3D RANSAC with MLE for finding inliers. The novelty of our algorithm is generalization of RANSAC in 3D. This algorithm modifies RANSAC in a way such that we look for the transformation that maximizes the likelihood function rather than maximizing the number of inliers. Our implementation of 3D MLESAC consists of the following basic steps.

Similar to 3D RANSAC, given N_{mlesac} iterations, in each iteration, five random components are sampled from the initial matching \mathcal{C} . We use these samples to calculate the affine transformation T and we transform all model keypoint that are in \mathcal{C} according to \mathcal{C} . We then define the likelihood function for each $i = 1, \dots, N$, with N being the number of column entries in \mathcal{C} as:

$$\Pr(d_i) = \gamma \frac{1}{\sqrt{2\pi\sigma^2}} \exp\left(-\frac{d_i^2}{2\sigma^2}\right) + (1 - \gamma) \frac{1}{\nu}, \quad (6)$$

where, d_i is the Euclidean distance between transformed model keypoints p_i with matched points p'_i in scene, ν is a constant, σ is the standard deviation, and γ is the mixing parameter, which has been calculated according to the method described in [18].

Since, distances d_i between p_i^S and $p_i^{S'}$ are independent of each other, the joint likelihood function for all d_i s given as:

$$\Pr(d) = \prod_{i=1}^N \left(\gamma \frac{1}{\sqrt{2\pi\sigma^2}} \exp\left(-\frac{d_i^2}{2\sigma^2}\right) + (1 - \gamma) \frac{1}{\nu} \right). \quad (7)$$

To simplify the calculations, we take logarithm on both sides of the above, giving the negative log-likelihood function as;

$$-L = -\sum_{i=1}^N \log \left(\gamma \frac{1}{\sqrt{2\pi\sigma^2}} \exp\left(-\frac{d_i^2}{2\sigma^2}\right) + (1 - \gamma) \frac{1}{\nu} \right). \quad (8)$$

Finally, the transformation that results in the minimum of negative log-likelihood function is compared with t_{mlesac} and it is considered the optimum transformation T^* . The correspondences in \mathcal{C} that do not agree with T^* are classified as outliers.

Note that the first term on the RHS of (6), refers to the correspondences that are inliers while the second term corresponds to the outliers, and is assumed to have a uniform distribution.

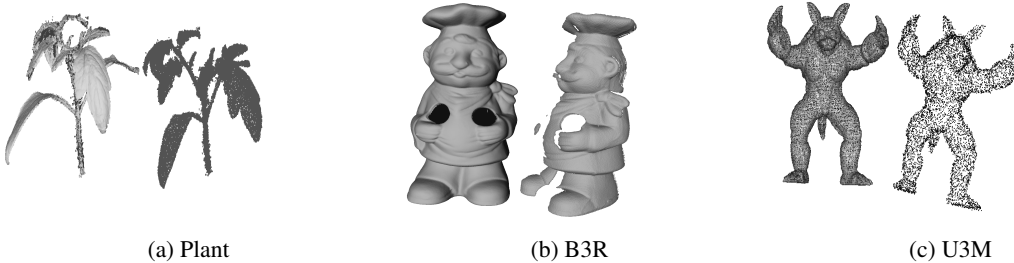


Figure 2: Visualization (snapshot) of sample model (right) and scene (left) from each dataset

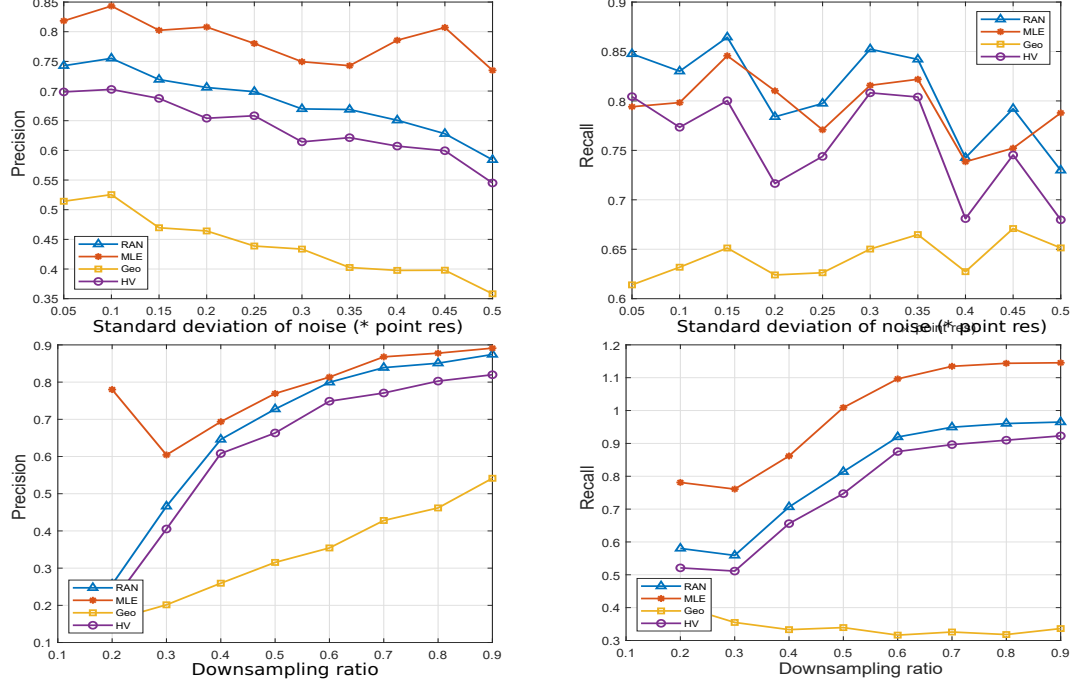


Figure 3: Performance of the evaluated CG algorithms in terms of precision and recall for the plant dataset

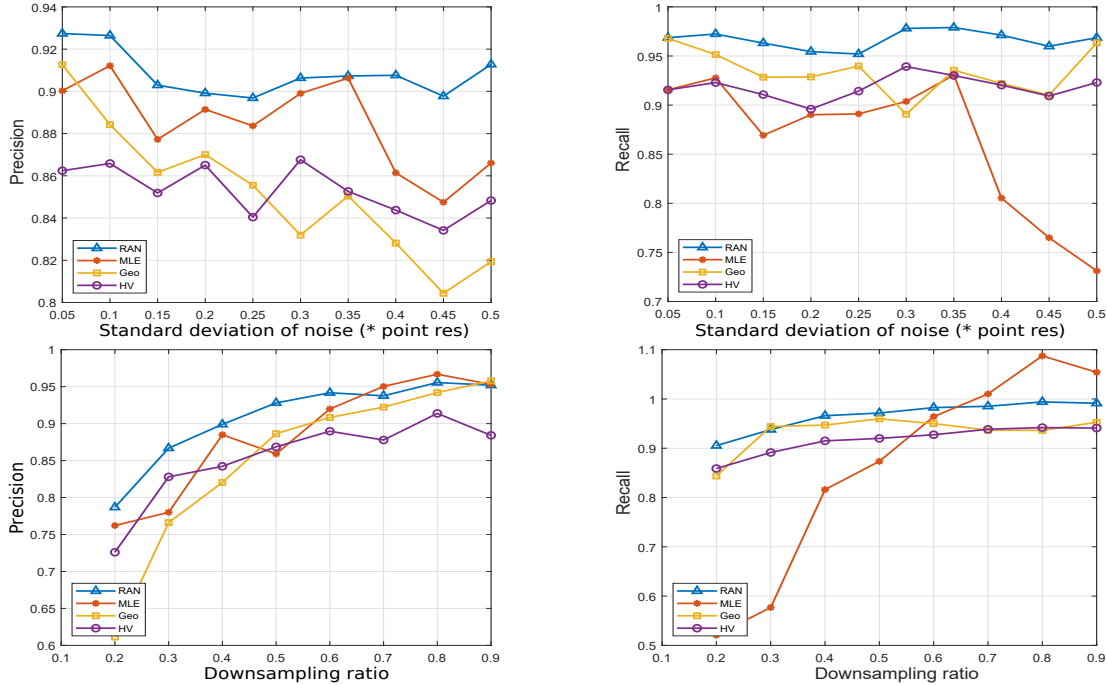


Figure 4: Performance of the evaluated CG algorithms in terms of precision and recall for the B3R dataset

4 Experimental evaluation and discussion

In this section, we evaluate and provide the implementation details of all the algorithms discussed in the previous section on two chosen benchmarks and a plant dataset. Fig.2 shows the samples of models and scenes in different datasets. These datasets have scenes with different noise levels, point densities, and partial overlaps. We determine the correctness of a correspondence using the ground truth affine transformation T_{GT} between the model and the scene. A

given correspondence c between points p, p' is declared correct if:

$$|\mathbf{T}_{GT}(p) - p'| \leq t, \quad (9)$$

Where t is the threshold. The calculated inliers by all algorithms are measured in terms of the *precision* and *recall* criteria which are defined in terms of the inlier set C_{in} , the correctly judged set C_{cor} , and the ground truth set C_{GT} as

$$\text{Precision} = \frac{|C_{cor}|}{|C_{in}|}, \quad (10)$$

and

$$\text{Recall} = \frac{|C_{cor}|}{|C_{GT}|}. \quad (11)$$

4.1 Dataset and experimental setup

4.1.1 Plant dataset

The models for this dataset have been obtained from the dataset containing 3D scans of plant shoot architectures provided by Salk Institute of Biological Science [25]. This dataset contains 559 3D plant shoot architectures from 4 species (Arabidopsis, tomato, tobacco, and sorghum) scanned under multiple conditions (ambient light (control), heat, high-light, shade, drought). Each plant was scanned every 1 or 2 days through roughly 20 days of development.

In our work we have used 26 model of sorghum, tobacco and tomato plants in three different conditions of control, shade and heat in different growth stage and different variety because this data has the same categories and the same number of replicates which makes it easier to compare the results. The scenes are created by rotating the models and by using different levels of noise and down-sampling on these models, giving a total of 80 scenes for each model under consideration.

4.1.2 B3R dataset

The Bologna 3D retrieval (B3R) dataset [26], with 6 models, is used to evaluation the algorithms robustness with respect to noise and point densities. The models are taken from the Stanford Repository, however the scenes here are created by rotating the models, and then adding 10 levels of noise and 8 levels of downsampling, giving a total of 80 scenes for each model.

Table 1: Implementation platforms of the used techniques

Technique	Platform
ISS Keypoints Detector	PCL
3D SIFT Descriptor	MATLAB
NNSR	MATLAB
RANSAC	MATLAB
GC	MATLAB
3D HV	MATLAB
3D MLESAC	MATLAB

Table 2: Parameters of algorithms

NNSR	t_{nnsr}	20		
RANSAC	t_{ransac}	0.01	N_{ran}	1000
GC	t_{GC}	0.01		
3D MLESAC	t_{mlesac}	0.01	N_{mlesac}	1000

4.1.3 U3M dataset

The UWA 3D modeling (U3M) [27] dataset belongs to the point cloud (2.5D view) registration scenario. There are 22, 16, 16 and 21 2.5D views respectively captured from the Chef, Chicken, T-rex, and Parasaurolophus models. There scenes represent different levels of overlaps. In our experiments, we have taken first 16 views of each model.

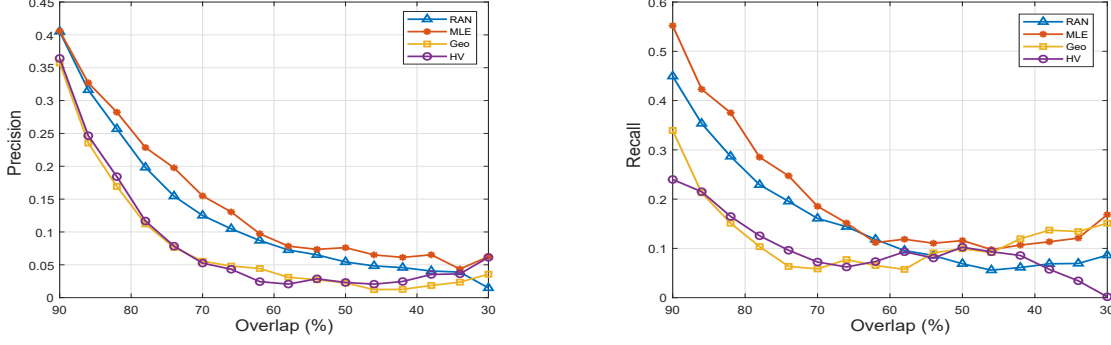


Figure 5: Performance of the evaluated CG algorithms in terms of precision and recall for the U3M dataset

4.1.4 Implementations details

In this paper, we have used 3D Intrinsic shape signature (ISS) for detecting keypoints and 3DSIFT for describing the local features. This choice is motivated by the results obtained in our previous work, where this detector-descriptor pair outperformed other combinations of popular detectors and descriptors in case of plant 3D point clouds. In the keypoint detection stage, around 3% of points in the point cloud are chosen as interest points, with the non maximum radius set to round 4 point cloud resolution (pr). For the 3DSIFT descriptor, the search radius is set to $8pr$ and the size of feature descriptor is 128. NNSR is used for finding initial matching. RANSAC, GC, 3DHV, and 3D MLESAC are used as 3DCG algorithms. Table.1 gives the implementation platforms of the used algorithms and the parameters used in all algorithms are listed in Table.2.

4.2 Results and discussions

4.2.1 Performance on the plant dataset

The performance of the 3DCG algorithms for the plant dataset are shown in Fig.3. Noise is expected to degrade on the discriminative capabilities of feature descriptor, thus creating a certain amount of false matches. This is obvious in the plots obtained for precision and recall for all the 3DCG algorithms. The precision decreases with increasing noise variance. Similar trend is observed for the recall values, however, the deterioration is smaller, as compared to the precision. Down sampling the scenes also has negative impact on the performance, as seen in the precision and recall plots. This can be attributed to the false matches that become more common as the number of points become less. As indicated by the plots, RANSAC and MLESAC appear to be the best two ones among all evaluated algorithms, considering their overall precision and recall performance, however, MLESAC generally outperforms RANSAC, while taking less time. This indicates that for larger point clouds of objects having highly complex shapes, MLESAC is a better choice as a 3DCG algorithm.

4.2.2 Performance on the B3R dataset

The performance of the 3DCG algorithms for the B3R dataset are shown in Fig.4. It follows similar trends, as in the case of the plant as seen in Fig.3. As indicated by the plots here also, RANSAC and MLESAC appear to be the best two ones among all evaluated algorithms, considering their overall precision and recall performance, with RANSAC performing slightly better. However, in our experiments, MLESAC is quite faster as compared to RANSAC.

4.2.3 Performance on the U3M dataset

A common trend to all algorithms is that their performance generally degrades as the degree of overlap drops as depicted in Fig.5. This is owing to the fact that the ratio of outliers in the initial correspondence set is closely correlated to the ratio of overlapping regions. MLESAC outperform in all algorithm in term of precious and recall.

4.2.4 Visualization

Fig.6 shows some visual results of 3DCG algorithms. These figures display the strength of each method. For example in NNSR method, The number of outliers are more than other methods, because of occlusion and overlap in the feature matching. We can also see the location and number of correspondences are also different.

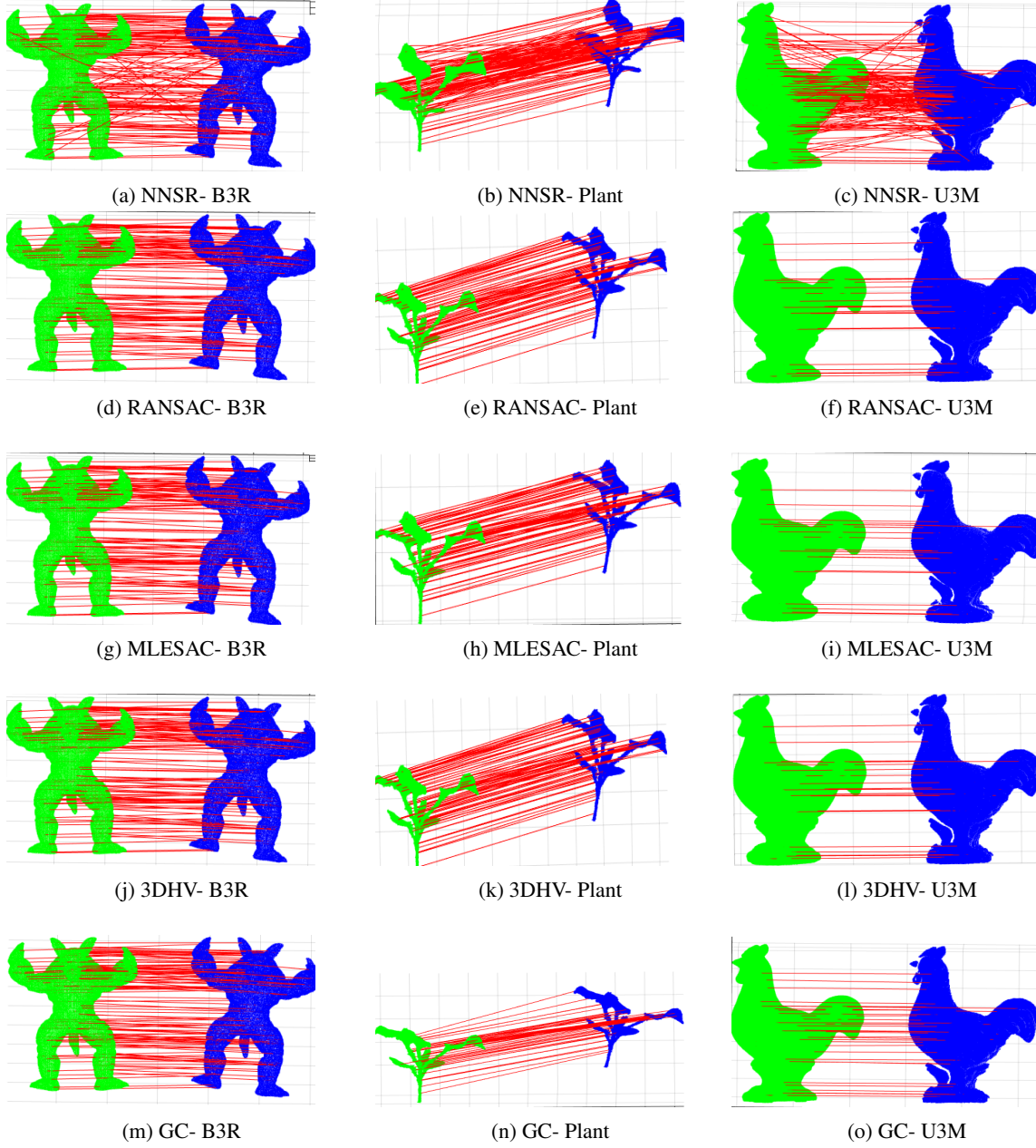


Figure 6: Visualization of the evaluated CG algorithms for the three datasets

5 Conclusions

In this paper, we compared the performance of different 3D correspondence grouping algorithms in context of 3D plant point clouds and also provided the corresponding performance evolution of some standard publically available datasets for comparison. The performance was evaluated in terms of precision and recall, the results were presented in terms of the corresponding plots. Experimental results show that the RANSAC and MLESAC perform quite closely and are better than 3D Hough Voting and Geometric Consistency. Also, in general, MLESAC is much faster compared to RANSAC, making it a better algorithm for applications involving 3D point clouds of plants as they are usually very large in size. In future works, we intend to prepare our own dataset of 3D point clouds of crops such as rice and wheat and will try to extend the analysis further to perform plant identification for plant phenomics applications.

References

- [1] Andrew J Challinor, J Watson, David B Lobell, SM Howden, DR Smith, and Netra Chhetri. A meta-analysis of crop yield under climate change and adaptation. *Nature Climate Change*, 4(4):287, 2014.
- [2] Noah Fahlgren, Malia A Gehan, and Ivan Baxter. Lights, camera, action: high-throughput plant phenotyping is ready for a close-up. *Current opinion in plant biology*, 24:93–99, 2015.
- [3] Massimo Minervini, Hanno Scharr, and Sotirios A Tsaftaris. Image analysis: the new bottleneck in plant phenotyping [applications corner]. *IEEE signal processing magazine*, 32(4):126–131, 2015.
- [4] Rachana Panwar, Kusha Goyal, Nilay Pandey, and Nitin Khanna. Imaging system for classification of local flora of uttarakhand region. In *2014 International Conference on Power, Control and Embedded Systems (ICPES)*, pages 1–6. IEEE, 2014.
- [5] Suxing Liu, Lucia Acosta-Gamboa, Xiuzhen Huang, and Argelia Lorence. Novel low cost 3d surface model reconstruction system for plant phenotyping. *Journal of Imaging*, 3(3):39, 2017.
- [6] Anders G Buch, Henrik G Petersen, and Norbert Krüger. Local shape feature fusion for improved matching, pose estimation and 3d object recognition. *SpringerPlus*, 5(1):297, 2016.
- [7] Huan Lei, Guang Jiang, and Long Quan. Fast descriptors and correspondence propagation for robust global point cloud registration. *IEEE Transactions on Image Processing*, 26(8):3614–3623, 2017.
- [8] Yu Xiang, Wongun Choi, Yuanqing Lin, and Silvio Savarese. Data-driven 3d voxel patterns for object category recognition. In *Proceedings of the IEEE Conference on Computer Vision and Pattern Recognition*, pages 1903–1911, 2015.
- [9] Anders Glent Buch, Yang Yang, Norbert Krüger, and Henrik Gordon Petersen. In search of inliers: 3d correspondence by local and global voting. In *Proceedings of the IEEE Conference on Computer Vision and Pattern Recognition*, pages 2067–2074, 2014.
- [10] Jiaqi Yang, Ke Xian, Yang Xiao, and Zhiguo Cao. Performance evaluation of 3d correspondence grouping algorithms. In *3D Vision (3DV), 2017 International Conference on*, pages 467–476. IEEE, 2017.
- [11] Marius Muja and David G Lowe. Fast matching of binary features. In *2012 Ninth conference on computer and robot vision*, pages 404–410. IEEE, 2012.
- [12] Antti Hietanen, Jussi Halme, Anders Glent Buch, Jyrki Latokartano, and J-K Kämäräinen. Robustifying correspondence based 6d object pose estimation. In *2017 IEEE International Conference on Robotics and Automation (ICRA)*, pages 739–745. IEEE, 2017.
- [13] Martin A Fischler and Robert C Bolles. Random sample consensus: a paradigm for model fitting with applications to image analysis and automated cartography. *Communications of the ACM*, 24(6):381–395, 1981.
- [14] Hui Chen and Bir Bhanu. 3d free-form object recognition in range images using local surface patches. *Pattern Recognition Letters*, 28(10):1252–1262, 2007.
- [15] Jiaqi Yang, Yang Xiao, Zhiguo Cao, and Weidong Yang. Ranking 3d feature correspondences via consistency voting. *Pattern Recognition Letters*, 117:1–8, 2019.
- [16] Federico Tombari and Luigi Di Stefano. Object recognition in 3d scenes with occlusions and clutter by hough voting. In *2010 Fourth Pacific-Rim Symposium on Image and Video Technology*, pages 349–355. IEEE, 2010.
- [17] Anders Glent Buch, Lilita Kiforenko, and Dirk Kraft. Rotational subgroup voting and pose clustering for robust 3d object recognition. In *2017 IEEE International Conference on Computer Vision (ICCV)*, pages 4137–4145. IEEE, 2017.

- [18] Philip HS Torr and Andrew Zisserman. Mlesac: A new robust estimator with application to estimating image geometry. *Computer vision and image understanding*, 78(1):138–156, 2000.
- [19] Lijin Deng, Yan Piao, and Shuo Liu. Research on sift image matching based on mlesac algorithm. In *Proceedings of the 2nd International Conference on Digital Signal Processing*, pages 17–21. ACM, 2018.
- [20] Lorenzo Torresani, Vladimir Kolmogorov, and Carsten Rother. Feature correspondence via graph matching: Models and global optimization. In *European Conference on Computer Vision*, pages 596–609. Springer, 2008.
- [21] David G Lowe. Distinctive image features from scale-invariant keypoints. *International journal of computer vision*, 60(2):91–110, 2004.
- [22] Chavdar Papazov and Darius Burschka. An efficient ransac for 3d object recognition in noisy and occluded scenes. In *Asian Conference on Computer Vision*, pages 135–148. Springer, 2010.
- [23] A Johnson and M Hebert. Surface matching for object recognition in complex 3-d scenes. to appear in. *Image and Vision Computing*, 1998.
- [24] Paul VC Hough. Method and means for recognizing complex patterns, December 18 1962. US Patent 3,069,654.
- [25] Saket Navlakha. 3d scans of plant shoot architectures, Jul 2017.
- [26] Federico Tombari, Samuele Salti, and Luigi Di Stefano. Performance evaluation of 3d keypoint detectors. *International Journal of Computer Vision*, 102(1-3):198–220, 2013.
- [27] Ajmal S Mian, Mohammed Bennamoun, and Robyn A Owens. A novel representation and feature matching algorithm for automatic pairwise registration of range images. *International Journal of Computer Vision*, 66(1):19–40, 2006.